High density nitrogen-vacancy sensing surface created via He^+ ion implantation of ^{12}C diamond

Ed E. Kleinsasser,[1,a)] Matthew M. Stanfield,[2] Jannel K. Q. Banks,[2] Zhouyang Zhu,[3,4] Wen-Di Li,[3,4] Victor M. Acosta,[5] Hideyuki Watanabe,[6] Kohei M. Itoh,[7] and Kai-Mei C. Fu[1,2,b)]
[1]*Department of Electrical Engineering, University of Washington, Seattle, Washington 98195-2500, USA*
[2]*Department of Physics, University of Washington, Seattle, Washington 98195-1560, USA*
[3]*HKU-Shenzhen Institute of Research and Innovation (HKU-SIRI), Shenzhen 518000, China*
[4]*Department of Mechanical Engineering, The University of Hong Kong, Pokfulam, Hong Kong, China*
[5]*Department of Physics and Astronomy, Center for High Technology Materials, University of New Mexico, Albuquerque, New Mexico 87106, USA*
[6]*Correlated Electronics Group, Electronics and Photonics Research Institute, National Institute of Advanced Industrial Science and Technology (AIST), Tsukuba Central 5, 1-1-1, Higashi, Tsukuba, Ibaraki 305-8565, Japan*
[7]*School of Fundamental Science and Technology, Keio University, 3-14-1 Hiyoshi, Kohoku-ku, Yokohama 223-8522, Japan*

(Received 3 February 2016; accepted 1 May 2016; published online 16 May 2016)

We present a promising method for creating high-density ensembles of nitrogen-vacancy centers with narrow spin-resonances for high-sensitivity magnetic imaging. Practically, narrow spin-resonance linewidths substantially reduce the optical and RF power requirements for ensemble-based sensing. The method combines isotope purified diamond growth, *in situ* nitrogen doping, and helium ion implantation to realize a 100 nm-thick sensing surface. The obtained $10^{17}\,cm^{-3}$ nitrogen-vacancy density is only a factor of 10 less than the highest densities reported to date, with an observed 200 kHz spin resonance linewidth over 10 times narrower. *Published by AIP Publishing.*
[http://dx.doi.org/10.1063/1.4949357]

The nitrogen-vacancy (NV) center in diamond is a versatile room-temperature magnetic sensor which can operate in a wide variety of modalities, from nanometer-scale imaging with single centers[1,2] to sub-picotesla sensitivities using ensembles.[3] Ensemble-based magnetic imaging, utilizing a two-dimensional array of NV centers,[4–6] combines relatively high spatial resolution with high magnetic sensitivity. These surfaces are ideal for imaging applications ranging from detecting magnetically tagged biological specimens[7,8] to fundamental studies of magnetic thin films.[9] A key challenge for array-based sensors is creating a high density of NV centers while still preserving the desirable NV spin properties. Here, we report on a promising method which combines isotope purified diamond growth, *in situ* nitrogen (N) doping, and helium ion implantation. In the 100 nm-thick sensor layer, we realize an NV density of $10^{17}\,cm^{-3}$ with a 200 kHz magnetic resonance linewidth. This corresponds to a DC magnetic sensitivity ranging from 170 nT (current experimental conditions) to 14 nT (optimized experimental conditions) for a 1 μm^2 pixel and 1 s measurement time.

Magnetic sensing utilizing NV centers is based on optically detected magnetic resonance (ODMR).[10–12] In the ideal shot-noise limit, the DC magnetic sensitivity is given by Ref. 9

$$\delta B_{\text{ideal}} \simeq \frac{h}{g\mu_B}\frac{1}{C}\frac{1}{\sqrt{\eta}}\sqrt{\frac{\delta\nu/\pi}{n_{NV}Vt}}, \tag{1}$$

in which $h/g\mu_B = 36\,\mu T/MHz$, C is the resonance dip contrast, η is the photon collection efficiency, $\delta\nu$ is the full-width at half maximum resonance linewidth, n_{NV} is the density of NV centers in imaging pixel volume V, and t is the measurement time. From Eq. (1), it is apparent that to minimize δB_{ideal} for a given linewidth $\delta\nu$, one would like to maximize the NV density n_{NV}. Increasing n_{NV}, however, can also increase $\delta\nu$. For example, lattice damage during the NV creation process can create inhomogeneous strain-fields.[13] More fundamentally, eventually NV-NV and NV-N dipolar interactions will contribute to line broadening. This dipolar broadening, $\delta\nu_{dp}$, is proportional to the nitrogen density n_N.[14,15] Since n_{NV} is typically proportional to n_N, we can divide $\delta\nu$ into two components, $\delta\nu = \delta\nu_0 + \delta\nu_{dp} = \delta\nu_0 + An_{NV}$, to obtain

$$\delta B_{\text{ideal}} \simeq \frac{h}{g\mu_B}\frac{1}{C}\frac{1}{\sqrt{\eta Vt\pi}}\sqrt{\frac{\delta\nu_0}{n_{NV}} + A}, \tag{2}$$

in which $\delta\nu_0$ depends on factors independent of NV density (e.g., hyperfine interaction with lattice nuclei, inhomogeneous strain fields). The second term A is due to the dipolar contribution to the linewidth and will depend on the ratio of n_N to n_{NV}. Equation (2) implies that the magnetic sensitivity improves significantly with density until $\delta\nu$ is dipolar limited. Thus, there is a threshold on the optimal NV density, $n_{\text{NV}} \gtrsim \delta\nu_0/A$.

There are practical reasons why, in the dipolar-broadened limit, it is beneficial to work at lower densities. By minimizing the ODMR linewidth, we minimize both the optical excitation (linear scaling with $\delta\nu$) and radio frequency (RF) power (quadratic scaling with $\delta\nu$) requirements for the measurement.[16] Additionally, reduced densities result in reduced photon count rates which maximize the measurement duty cycle, minimizing detector dead time/readout time. Thus, a

a)edklein@uw.edu
b)kaimeifu@uw.edu

reasonable method to optimize δB is to first minimize $\delta\nu_0$ and then increase n_{NV} until the density independent and dipolar contributions to the sensitivity become comparable.

To minimize $\delta\nu_0$, this work utilizes nitrogen that is incorporated *in situ* during diamond growth via chemical vapor deposition (CVD) on a (100)-oriented electronic grade substrate (Element Six, $n_{N,substrate} < 1$ ppb). *In situ* doping theoretically enables uniform-in-depth nitrogen incorporation in the 100 nm thick sensor while avoiding lattice damage caused by (more standard) nitrogen ion implantation. Additionally, we utilize isotopically purified ^{12}C to eliminate $\delta\nu$ broadening due to the NV hyperfine coupling to ^{13}C.[17,18]

Next, the sample was implanted with He^+ ions in arrays of $5 \times 5\ \mu m$ squares to create lattice vacancies. Different implantation conditions were tested with ion doses ranging from 10^9–$10^{13}\,cm^{-2}$ at acceleration voltages of 15, 25, and 35 keV. After implanting, the sample was annealed at 850 °C for 1.5 h in an Ar/H_2 forming gas to allow the vacancies to diffuse to the doped nitrogen to form NV centers. A second 24 h anneal at 450 °C in air was performed to convert NV centers from the neutral (NV^0) to the negative (NV^-) charge state.[19] He^+ implantation into a uniformly N-doped layer, followed by annealing, produces a uniform layer of NV centers with a controllable sensor thickness. The method also provides independent handles on both nitrogen and vacancy densities to optimize NV formation. This is impossible with N^+ implantation alone where typically dozens of vacancies are created for every implanted N^+ ion.

To characterize the NV^- density, photoluminescence (PL) intensity from the He^+ implanted squares was compared to an average of single, near-surface NV centers in a control sample. The 2D density was calculated with the known excitation spot size and converted to a 3D density by assuming a uniform distribution of NV centers throughout the 100 nm thick N-doped layer. As only the negatively charged state of the NV center is useful for magnetic sensing, room temperature PL spectra were used to confirm the synthesized centers were in the desired charge state.

Before He^+ implanting and annealing, the density of NV centers formed during growth was in the range of 0.7–3 $\times 10^{15}\,cm^{-3}$ (average value $1.5 \times 10^{15}\,cm^{-3}$). The range in density is due to uneven incorporation of nitrogen during CVD growth which will be discussed further below. Figure 1 shows an NV^- density map, after annealing, of three squares implanted with 10^{11}, 10^{12}, and $10^{13}\,cm^{-2}$ He^+ ions at 15 keV. Experimentally we found that n_{NV} for the three acceleration voltages varied by less than a factor of 2. This is consistent with simulations[20] which show an average number of vacancies produced per ion of 30, 36, and 39, and an average ion range of 72, 112, and 135 nm, for 15, 25, and 35 keV acceleration voltages, respectively. All stopping ranges are within the 200 nm vacancy diffusion length[21] of the 100 nm N-doped layer.

During the implantation process, the entire sample was exposed to an unknown He^+ radiation dose resulting in a background NV concentration of $0.1–1 \times 10^{16}\,cm^{-3}$. Squares implanted with ion doses of 10^9 and $10^{10}\,cm^{-2}$ were indistinguishable from this background in most of the implanted areas. The optimal ion dose was $10^{12}\,cm^{-2}$ resulting in an average n_{NV} of $1 \times 10^{17}\,cm^{-3}$ which corresponds to a 60-fold

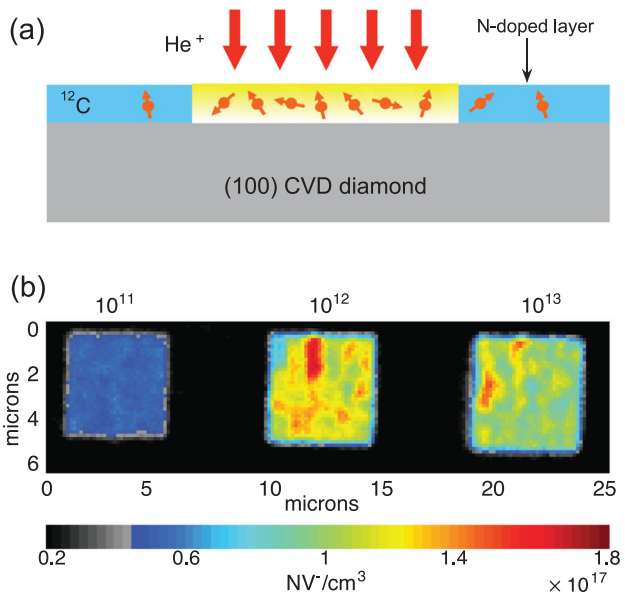

FIG. 1. (a) Schematic of the diamond sample illustrating the 100 nm ^{12}C isotopically pure layer implanted with He^+ ions. (b) Confocal scan of $(5\ \mu m)^2$ implanted squares. Excitation at 532 nm with 1 mW power, collection band from 650 to 800 nm. From left to right, the squares were implanted with ion doses of 10^{11}, 10^{12}, and $10^{13}\,cm^{-2}$ at an acceleration voltage of 15 keV.

increase in n_{NV} over the unimplanted case. The obtained density is only one order of magnitude lower than the highest densities reported.[11,22] These very high densities were obtained in high nitrogen doped (>100 ppm) diamond which exhibits significantly broader resonance lines (2 MHz),[11] where the dominant contribution is due to N-NV dipolar coupling.[16] Densities of $10^{17}\,cm^{-3}$ have also been obtained with N implantation and annealing[23] which also exhibited several MHz linewidths.

Room-temperature spectra comparing the NV^- zero-phonon-line photoluminescence intensities for the implanted and unimplanted cases show a similar increase (~40-fold) in NV density for the optimal implantation dose, as shown in Fig. 2(a). Figure 2(b) shows the ratio of NV^- to total NV ($NV^- + NV^0$) for different optical powers. The high ratio at low intensities indicates the NV centers are predominately in the desired charge state in the absence of optical excitation. The decrease in ratio with increased power is consistent with photoionization effects reported previously.[24]

Next, we measured the ODMR linewidth, $\delta\nu$, of the doped layer. Figure 3(a) shows an (ODMR) spectrum for the $m_s = 0 \leftrightarrow m_s = -1$ transition for one of the four NV crystal orientations. During the measurement, the NV centers are excited using a 532 nm continuous-wave (CW) laser, while an RF field is swept through the electron spin resonance. Three dips are observed due to the hyperfine interaction of the NV electronic state with the ^{14}N nucleus.[11] To determine $\delta\nu$, the ODMR fluorescence spectra were fit to the sum of three Lorentzian functions of equal amplitude and $\delta\nu$, with a fixed 2.17 MHz hyperfine splitting.

Figure 3(b) shows a plot of $\delta\nu$ vs. microwave power for the unimplanted and implanted conditions (15 keV, $10^{12}\,cm^{-2}$). The data are fit to the theoretical model $\delta\nu = \delta\nu_{RF=0} + b\sqrt{P_{RF}}$, where $\delta\nu_{RF=0}$ is the intrinsic dephasing rate, P_{RF} is the applied RF power, and b is a constant scaling

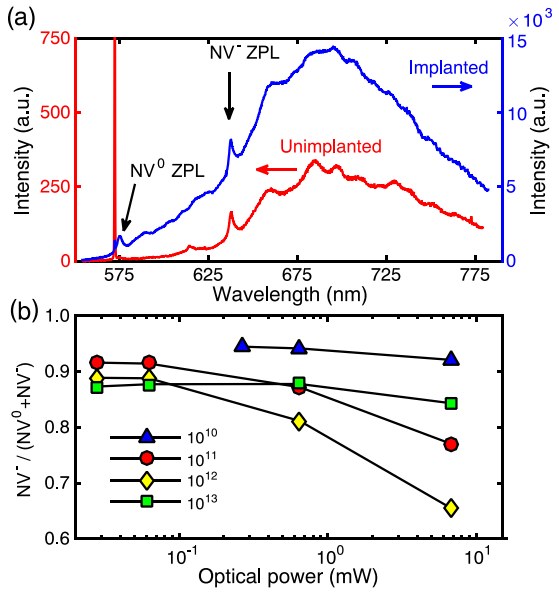

FIG. 2. (a) Spectra of unimplanted and implanted conditions illustrating the increase in photoluminescence after He^+ implanting (15 keV, 10^{12} cm^{-2}). Excitation at 532 nm with 1 mW power. (b) Plot of the ratio of NV^- to total NV vs. optical power. For the ratio, the difference in the relative weight of the NV^0 and NV^- ZPL due to the different Huang-Rhys factors (approximately a factor of 2) has been taken into account.[25,26]

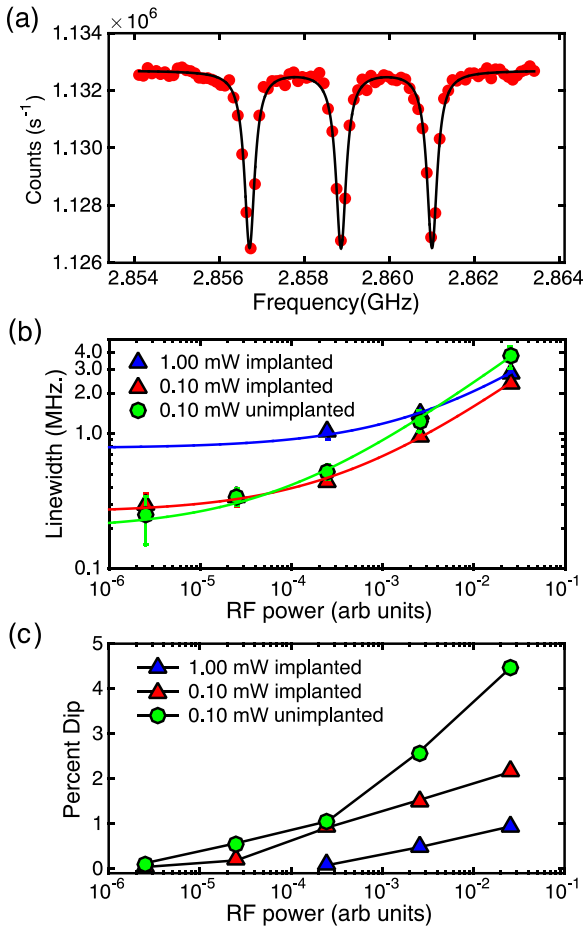

FIG. 3. (a) ODMR scan of an implanted square with $\delta\nu = 290$ kHz excited with 78 μW/μm^2 of optical power. (b) Measured linewidth ($\delta\nu$) vs. RF power. The error bars signify the 95% confidence interval of the width parameter for the Lorentzian fit function. (c) Optical contrast (depth of the resonance dip) vs. microwave power for unimplanted and implanted (15 keV, 10^{12} cm^{-2}) conditions.

to account for RF power broadening. The inhomogeneous spin relaxation time, $T_2^* = 1/(\pi\delta\nu_{RF=0})$, is determined from this fit. Experimentally we found that optical excitation powers below 100 μW did not affect T_2^*. No measurable difference in T_2^* was found between the unimplanted and 15 keV implantation cases, which both exhibit T_2^* of 1.5 μs ($\delta\nu \cong 200$ kHz). As little improvement in NV density was observed for higher implantation energies, detailed T_2^* data for implantation energies greater than 15 keV were not taken.

The observed 200 kHz linewidth for our dense ensemble of NV centers is similar to ensembles created via electron irradiation of 1 ppm N bulk ^{12}C diamond,[27] and 2–5 times narrower than naturally abundant diamond.[11,28] This suggests that there is a significant benefit in utilizing isotope purified ^{12}C for He^+ implanted samples. The 200 kHz linewidth is significantly broader than the 10 kHz inhomogeneous linewidth demonstrated in low-nitrogen ^{12}C diamond,[29] which was limited by variations in the microscopic strain in the sample.[9] Given the minimal difference in T_2^* for unimplanted vs. implanted conditions, we attribute the dominant dephasing mechanism to dipolar interactions between the NV centers and native nitrogen.

A critical parameter which affects magnetometry performance is the ratio of n_{NV} to the density of all other paramagnetic impurities. Assuming the latter is dominated by unconverted substitutional nitrogen, then the relevant quantity is $n_{NV}/(n_{N+NV})$. We can estimate this ratio using two different methods. First, for CVD diamond grown on a (100) substrate, the initial ratio of $n_N : n_{NV}$ is typically found to be 100:(0.2–0.5).[30] After helium ion implantation and annealing, the NV density increased by 40–60 times, suggesting that $n_{NV}/(n_{N+NV})$ ranges from 8% to 30%. Alternatively, we can directly use the ESR linewidth. We again assume the dominate contribution to the linewidth is the dipolar coupling between the NV and substitutional nitrogen. The ESR linewidth of the spin 1/2 substitutional nitrogen interacting with the nitrogen bath is known to be $\delta\nu = 3.1 \times 10^4 f_N$ (Hz/ppm),[14] where f_N is the nitrogen concentration in ppm. Given the similar gyromagnetic ratio for N and NV, we can use this experimental linewidth to estimate the linewidth of an NV center interacting with a N bath. This results in $f_N = 6.4$ ppm for a 200 kHz linewidth and $n_{NV}/(n_{N+NV}) = 8\%$ which is consistent with the former estimate.

We now estimate the DC magnetic sensitivity of the engineered layer for a 1 s integration time. For a sensor biased at the steepest slope of the ODMR curve, the shot-noise magnetic sensitivity is given by[9]

$$\delta B_{\mathrm{sn,cw}} \simeq \frac{h}{g\mu_B}\frac{1}{C}\frac{\delta\nu}{\sqrt{I_0 t}}, \tag{3}$$

in which I_0 is the detected photon count rate from the NV centers in the measurement pixel. For the case of continuous-wave (CW) RF and optical fields, the realized sensitivity is a complex interplay between optical and RF power. The optical excitation power has counteracting effects on $\delta B_{\mathrm{sn,cw}}$, both increasing I_0 and, typically, $\delta\nu$ (Fig. 3(b)). Similarly, increasing the RF power will both increase $\delta\nu$ and C (Fig. 3(c)). For

a $1\,\mu m^2$ pixel, we find a sensitivity of $\delta B_{sn,cw} \simeq 170\,nT$ at $100\,\mu W$ optical excitation power and an RF power corresponding to $C = 0.01$. This can be readily improved by a factor of $\sqrt{3}$ utilizing a high-NA objective[31] and a further factor of 3 by driving all three hyperfine transitions simultaneously, resulting in a sensitivity of $\delta B_{sn,\,cw} \simeq 30\,nT$.

The sensitivity can be further improved utilizing pulsed techniques. In this case, we can decouple the optical excitation from the spin manipulation, enabling the use of high optical powers for spin readout without adversely affecting the ODMR linewidth. The optimal spin-manipulation time is $\approx T_2^*$,[15] resulting in a time-averaged photon count rate of $I_0 \rightarrow I_0\tau_L/(T_2^* + \tau_{init} + \tau_L)$ in Eq. (3), in which τ_L is the optical read-out pulse length and τ_{init} is the initialization time.[9] The pulsed sensitivity is given by

$$\delta B_{sn,pulsed} \simeq \frac{h}{g\mu_B}\frac{\delta\nu}{C}\frac{\sqrt{1/\pi\delta\nu + \tau_{init} + \tau_L}}{\sqrt{I_0\tau_L t}}, \qquad (4)$$

which reduces to Eq. (1) in the limit that $T_2^* \gg (\tau_{init} + \tau_L)$. Using reasonable parameters ($\tau_L = 300\,ns$, $\tau_{init} = 1\,\mu s$, $C = 0.05$, $I_0 = n_{NV}\,V \times 10^5$ counts s^{-1} (Ref. 31)), we estimate a sensitivity of $\delta B_{sn,pulsed} \simeq 14\,nT$. We note that most ensembles experiments work in the regime in which $T_2^* \ll (\tau_{init} + \tau_L)$ which results in $\delta B \propto (T_2^*\sqrt{I_0})^{-1} \propto \sqrt{1/T_2^*} \propto \sqrt{n_{NV}}$. In this duty-cycle limited regime, it is still advantageous to increase T_2^* even in the dipolar-broadened limit. By raising T_2^* to $1.5\,\mu s$, which is comparable to typical choices for $(\tau_{init} + \tau_L)$, we make significant step toward suppressing this duty cycle issue and reaching the fundamental ensemble DC sensitivity.

In future sensors, optimizing the initial nitrogen density n_N such that $\delta\nu_0 \approx \delta\nu_{dp} \approx 10\,kHz$ could result in a further ~10-fold decrease in the ODMR linewidth. More critically, however, is the need to further improve the uniformity of N incorporation during CVD growth. In this work, initial nitrogen incorporation densities varied by a factor of 3–4. Theoretically, in a calibrated, stable imaging system, this deviation should not pose a problem. Practically, however, spatial variations over time (e.g., due to vibrations or thermal drift) will result in a false magnetic signal. It has been recognized that nitrogen incorporation during diamond growth is extremely sensitive to the growth plane[32,33] and thus surface steps on a (100) surface. By reducing the misorientation of the surface cut (typically 1% in our samples), we expect to be able to enhance the incorporation homogeneity. High NV spatial uniformity combined with the realized optical and spin properties presented in this work is expected to result in a high-sensitivity magnetic imaging system for magnetically tagged biological applications and the study of optical-scale magnetic phenomena.

This work has been supported by a University of Washington Molecular Engineering and Sciences Partnership grant. The work at Keio University has been supported by JSPS KAKENHI (S) No. 26220602 and Core-to-Core Program. V.M.A. acknowledges support from NSF Grant No. IIP-1549836 and valuable conversations with J. Barry. W.D.L. was sponsored by NSF of China (Grant No. 61306123) and RGC of HKSAR (Grant No. 27205515). Z.Z. and W.D.L. thank the facility support from Nanjing National Laboratory of Microstructures.

[1]G. Balasubramanian, I. Chan, R. Kolesov, M. Al-Hmoud, J. Tisler, C. Shin, C. Kim, A. Wojcik, P. R. Hemmer, A. Krueger *et al.*, Nature **455**, 648 (2008).
[2]J. Maze, P. Stanwix, J. Hodges, S. Hong, J. Taylor, P. Cappellaro, L. Jiang, M. G. Dutt, E. Togan, A. Zibrov *et al.*, Nature **455**, 644 (2008).
[3]T. Wolf, P. Neumann, K. Nakamura, H. Sumiya, T. Ohshima, J. Isoya, and J. Wrachtrup, Phys. Rev. X **5**, 041001 (2015).
[4]S. Steinert, F. Dolde, P. Neumann, A. Aird, B. Naydenov, G. Balasubramanian, F. Jelezko, and J. Wrachtrup, Rev. Sci. Instrum. **81**, 043705 (2010).
[5]B. Maertz, A. Wijnheijmer, G. Fuchs, M. Nowakowski, and D. Awschalom, Appl. Phys. Lett. **96**, 092504 (2010).
[6]L. M. Pham, D. Le Sage, P. L. Stanwix, T. K. Yeung, D. Glenn, A. Trifonov, P. Cappellaro, P. Hemmer, M. D. Lukin, H. Park *et al.*, New J. Phys. **13**, 045021 (2011).
[7]M. Gould, R. J. Barbour, N. Thomas, H. Arami, K. M. Krishnan, and K.-M. C. Fu, Appl. Phys. Lett. **105**, 072406 (2014).
[8]D. R. Glenn, K. Lee, H. Park, R. Weissleder, A. Yacoby, M. D. Lukin, H. Lee, R. L. Walsworth, and C. B. Connolly, Nat. Methods **12**, 736 (2015).
[9]L. Rondin, J. Tetienne, T. Hingant, J. Roch, P. Maletinsky, and V. Jacques, Rep. Prog. Phys. **77**, 056503 (2014).
[10]D. Budker and M. Romalis, Nat. Phys. **3**, 227 (2007).
[11]V. Acosta, E. Bauch, M. Ledbetter, C. Santori, K.-M. Fu, P. Barclay, R. Beausoleil, H. Linget, J. Roch, F. Treussart *et al.*, Phys. Rev. B **80**, 115202 (2009).
[12]N. Manson, J. Harrison, and M. Sellars, Phys. Rev. B **74**, 104303 (2006).
[13]K. Fang, V. M. Acosta, C. Santori, Z. Huang, K. M. Itoh, H. Watanabe, S. Shikata, and R. G. Beausoleil, Phys. Rev. Lett. **110**, 130802 (2013).
[14]J. Van Wyk, E. Reynhardt, G. High, and I. Kiflawi, J. Phys. D: Appl. Phys. **30**, 1790 (1997).
[15]J. Taylor, P. Cappellaro, L. Childress, L. Jiang, D. Budker, P. Hemmer, A. Yacoby, R. Walsworth, and M. Lukin, Nat. Phys. **4**, 810 (2008).
[16]P. Kehayias, M. Mrózek, V. Acosta, A. Jarmola, D. Rudnicki, R. Folman, W. Gawlik, and D. Budker, Phys. Rev. B **89**, 245202 (2014).
[17]K. Ohashi, T. Rosskopf, H. Watanabe, M. Loretz, Y. Tao, R. Hauert, S. Tomizawa, T. Ishikawa, J. Ishi-Hayase, S. Shikata, C. Degen, and K. Itoh, Nano Lett. **13**, 4733 (2013).
[18]K. Itoh and H. Watanabe, MRS Commun. **4**, 143 (2014).
[19]K.-M. Fu, C. Santori, P. Barclay, and R. Beausoleil, Appl. Phys. Lett. **96**, 121907 (2010).
[20]J. F. Zieglera, M. D. Zieglerb, and J. P. Biersackc, Nucl. Instrum. Meth. B **268**, 1818–1823 (2010).
[21]C. Santori, P. E. Barclay, K.-M. C. Fu, and R. G. Beausoleil, Phys. Rev. B **79**, 125313 (2009).
[22]J. Botsoa, T. Sauvage, M.-P. Adam, P. Desgardin, E. Leoni, B. Courtois, F. Treussart, and M.-F. Barthe, Phys. Rev. B **84**, 125209 (2011).
[23]A. Waxman, Y. Schlussel, D. Groswasser, V. Acosta, L.-S. Bouchard, D. Budker, and R. Folman, Phys. Rev. B **89**, 054509 (2014).
[24]N. Manson and J. Harrison, Diamond Relat. Mater. **14**, 1705 (2005).
[25]G. Davies and M. Crossfield, J. Phys. C: Solid State Phys. **6**, L104 (1973).
[26]A. Alkauskas, B. B. Buckley, D. D. Awschalom, and C. G. Van de Walle, New J. Phys. **16**, 073026 (2014).
[27]C. Grezes, B. Julsgaard, Y. Kubo, W. Ma, M. Stern, A. Bienfait, K. Nakamura, J. Isoya, S. Onoda, T. Ohshima *et al.*, Phys. Rev. A **92**, 020301 (2015).
[28]V. M. Acosta, K. Jensen, C. Santori, D. Budker, and R. G. Beausoleil, Phys. Rev. Lett. **110**, 213605 (2013).
[29]T. Ishikawa, K.-M. C. Fu, C. Santori, V. M. Acosta, R. G. Beausoleil, H. Watanabe, S. Shikata, and K. M. Itoh, Nano Lett. **12**, 2083 (2012).
[30]A. Edmonds, U. D'Haenens-Johansson, R. Cruddace, M. Newton, K.-M. Fu, C. Santori, R. Beausoleil, D. Twitchen, and M. Markham, Phys. Rev. B **86**, 035201 (2012).
[31]F. Jelezko and J. Wrachtrup, Phys. Status Solidi A **203**, 3207 (2006).
[32]R. Samlenski, C. Haug, R. Brenn, C. Wild, R. Locher, and P. Koidl, Appl. Phys. Lett. **67**, 2798 (1995).
[33]T. Miyazaki, Y. Miyamoto, T. Makino, H. Kato, S. Yamasaki, Y. Fukui, Y. Doi, N. Tokuda, M. Hatano, and N. Mizuochi, Appl. Phys. Lett. **105**, 261601 (2014).